PHYSICAL REVIEW A VOLUME 60, NUMBER 6 DECEMBER 1999

Photoionization of Fe XV

Nasreen Haque
Department of Physics, Morehouse College, Atlanta, Georgia 30314

Anil K. Pradhan
Department of Astronomy, The Ohio State University, Columbus, Ohio 43210

(Received 26 August 1999)

Relativistic and resonance effects in the photoionization of Mg-like Fe XV are investigated using the Breit-Pauli *R*-matrix method at near-threshold and intermediate energies, complemented by the relativistic random-phase approximation and multichannel quantum-defect theory in the energy region up to the *L*-shell ionization thresholds. The cross sections exhibit extensive resonance structures that considerably enhance the effective photoionization of Fe XV. These results should be of general interest in photoionization modeling of x-ray sources observed by space observatories. [S1050-2947(99)51012-3]

PACS number(s): 32.80.Fb, 32.30.Rj, 98.58.Bz, 98.70.Qy

There is particular interest in the photoionization of highly charged iron ions owing to their importance in the modeling of astrophysical plasmas such as in active galactic nuclei and quasars, supernovae, stellar coronae, etc., and in laboratory sources such as inertial and magnetic confinement fusion devices [1]. Among the most complex atomic species are those that are isoelectronic with the third row elements containing open $n=3$ shells. The *K*- and *L*-shell photoexcitations and photoionizations are highly topical areas of investigation, as they are generally in the x-ray range accessible to satellite observations, such as from the recently launched Chandra X-ray Observatory (CXO), and the upcoming X-ray Multi-Mirror Mission (XMM) and Astro-E [1].

While previous calculations exist for the iron ions, they are in relatively simpler approximations that neglect the multiplet or the fine structure, and autoionizing resonances that are known to enhance the cross sections significantly [2]. Recently, extensive photoionization calculations were carried out in the close-coupling approximation using the *R*-matrix method under the Opacity Project (OP) [3] for most astrophysically abundant elements. While the OP cross sections include the resonance effects, in *LS* coupling they neglect fine-structure effects in the detailed cross sections, as shown in this work through relativistic close-coupling calculations using the Breit-Pauli *R*-matrix codes developed for the Iron Project [4].

Whereas the low-energy region can be accurately considered with the Breit-Pauli *R*-matrix method (BPRM) method, at higher energies leading up to the *L*- and *K*-shell ionization the number of coupled channels becomes very large and the computations quite prohibitive. On the other hand, there are very few studies done of the resonance structures leading up to these ionization edges [5]. It is therefore of interest to not only carry out the low-energy BPRM calculations, but also to study the nature of resonances at high energies using other methods such as the relativistic random-phase approximation (RRPA) and relativistic multichannel quantum-defect theory (RMQDT). The aim is to combine the two techniques to investigate photoionization cross sections over the entire energy range of practical interest, as a guide to more elaborate close-coupling calculations.

The computationally intensive BPRM calculations are carried out as described in recent works [6]. The residual (target) ion following photoionization is represented by an *N*-electron system, and the total wave function of the initial bound $(N+1)$ electron-ion system is represented in terms of the ion eigenfunctions as

$$\Psi(E)=A\sum_i \chi_i\theta_i+\sum_j c_j\Phi_j, \qquad (1)$$

where χ_i is the ion wave function in a specific state $S_iL_iJ_i\pi_i$ and θ_i is the wave function for the $(N+1)$-th electron in a channel labeled as $S_iL_i(J_i)\pi_ik_i^2\ell_i[J\pi]$; k_i^2 being its incident kinetic energy. The Φ_j's are the correlation functions of the $(N+1)$-electron system that account for short-range correlation and the orthogonality between the continuum and the bound orbitals. The Φ_j's may also give rise to bound channel resonances at intermediate energies due to inner-shell photoexcitation autoionization, as described in this work.

The eigenfunctions χ_i of the residual ion Fe XVI are obtained through atomic-structure calculations using the program SUPERSTRUCTURE [7]. Table I lists the χ_i corresponding to 17 levels dominated by configurations $2p^6(^1S)n\ell$, up to $n=5$. The calculated eigenenergies are compared with the experimental values. Although the Fe XVI levels included in the close-coupling expansion span the $n=5$ levels, most of the relevant resonance structure appears below the first excited fine-structure levels $^2P_0$1/2,3/2. However, owing to the high ion charge the *n* complexes are well separated and the coupling effects, including resonances at higher energies, are weak.

We consider the photoionization of the ground level of Fe XV, $3s^2(^1S_0)+h\nu\rightarrow e+3s(^2S_{1/2})$, coupled to the continua of the ground and the excited levels of Fe XVI. Figure 1 shows the detailed cross section with the Rydberg series of resonances in the region up to, and slightly above, the first two excited thresholds $3p(^2P^o_{1/2,3/2})$. For comparison, the nonrelativistic cross sections from the Opacity Project work by Butler *et al.* [8] are also shown (dashed lines). It is seen that the OP results, in *LS* coupling, did not resolve the extensive resonance structures obtained in the present calcula-

TABLE I. Fe XVI target level energies (Ry) in the wave-function expansion.

Index	Configuration [Term]	J	E(Obs.)	E(Calc.)
1	$2p^6(^1S)3s\ [^2S]$	1/2	0.000 00	0.000 00
2	$2p^6(^1S)3p\ [^2P^o]$	1/2	2.525 96	2.521 86
3	$2p^6(^1S)3p\ [^2P^o]$	3/2	2.716 88	2.690 95
4	$2p^6(^1S)3d\ [^2D]$	3/2	6.155 44	6.216 37
5	$2p^6(^1S)3d\ [^2D]$	5/2	6.181 98	6.254 59
6	$2p^6(^1S)4s\ [^2S]$	1/2	17.0182	17.0836
7	$2p^6(^1S)4p\ [^2P^o]$	1/2	18.0252	18.0643
8	$2p^6(^1S)4p\ [^2P^o]$	3/2	18.0980	18.1269
9	$2p^6(^1S)4d\ [^2D]$	3/2	19.3570	19.4013
10	$2p^6(^1S)4d\ [^2D]$	5/2	19.3677	19.4186
11	$2p^6(^1S)4f\ [^2F^o]$	5/2	19.9077	19.9638
12	$2p^6(^1S)4f\ [^2F^o]$	7/2	19.9125	19.9703
13	$2p^6(^1S)5s\ [^2S]$	1/2	24.2500	24.3164
14	$2p^6(^1S)5p\ [^2P^o]$	1/2	24.7606	24.8020
15	$2p^6(^1S)5p\ [^2P^o]$	3/2	24.7970	24.8357
16	$2p^6(^1S)5d\ [^2D]$	3/2	25.4065	25.4552
17	$2p^6(^1S)4d\ [^2D]$	5/2	25.4116	25.4639

tions including relativistic fine structure. In the region $^2P^o_{1/2}$-$^2P^o_{3/2}$ the resonances are considerably weaker than in the region below the $^2P^o_{1/2}$ owing to autoionization into the excited $3p\ ^2P^o_{1/2}$ continuum, in addition to the ground level continuum $3s(^2S_{1/2})$. Figure 2 shows the photoionization cross section in an extended energy range that spans all excited Fe XVI levels in the close-coupling expansion (Table I). Above the $3p\ ^2P^o_{1/2,3/2}$ thresholds however, resonance structures are fairly isolated and relatively far apart. The background cross sections and some resonance positions agree well with the earlier LS coupling OP results [8].

BPRM calculations can be further extended in the intermediate energy range, from the highest target level to the $n=2$ inner-shell ionization thresholds. This region does not include the target levels that would correspond to the first sum in the close-coupling expansion [Eq. (1)]. However, a number of $(N+1)$-electron configurations, Φ_j(Fe XV), are included in the BPRM calculations in the second sum in Eq. [1]) with eigenvalues in this range. These Fe XV configurations correspond to outer $3s$ electron excitation, as well as the inner $2p$ electron excitations, i.e., $[1s^22s^22p^6]3\ell^2+3\ell,n\ell$; $n\leqslant 5,\ell\leqslant 2$, and the inner-shell excitation configurations: $[1s^22s^22p^5]3\ell^2n\ell$; $n\leqslant 5,\ell\leqslant 2$. Although the $2p$-shell ionizations are not explicitly represented in the BPRM calculations, the $2p$-shell excitation autoionization is included to some extent via resonances corresponding to these Φ_j(Fe XV). Some of the resonances in the 30–80 Ry region, due to inner-shell photoexcitations, are much stronger than those due to the valence $3s$-shell excitations in Figs. 1 and 2, as discussed below (Fig. 4).

Close to the ionization threshold of the $n=2$, we carry out RRPA+RMQDT calculations, with the detailed resonance strucutures shown in Fig. 3. The RRPA and RMQDT calculations are carried out as described in [9] and [10]. In the autoionization resonance spectrum region between 80 and 86 Ry, the photoionization cross section in open dissociation channels, that is, the $3s$ photoionization cross section, is calculated and plotted as a function of photon energy in Fig. 3. The seven interacting relativistic dipole channels considered for the RRPA+RMQDT calculations are $3s\rightarrow\epsilon(p_{3/2}),\epsilon(p_{1/2})$; $2p3/2\rightarrow nd_{5/2,3/2},ns_{1/2}$; and $2p_{1/2}\rightarrow nd_{3/2},ns_{1/2}$. The theoretical single-configuration Dirac-Fock thresholds for $3s,2p_{3/2},2p_{1/2}$ are at 33.314, 86.26, and 87.21 Ry, respectively. Below the $2p_{3/2}$ threshold there are five interacting Rydberg series corresponding to discrete excitation from $2p_{3/2}$ and $2p_{1/2}$ levels. Coupling between these excitation channels and the ionization channels from the $3s$ levels causes configuration interaction between the discrete and continuum states, which in turn leads to autoionization resonances seen in Fig. 3.

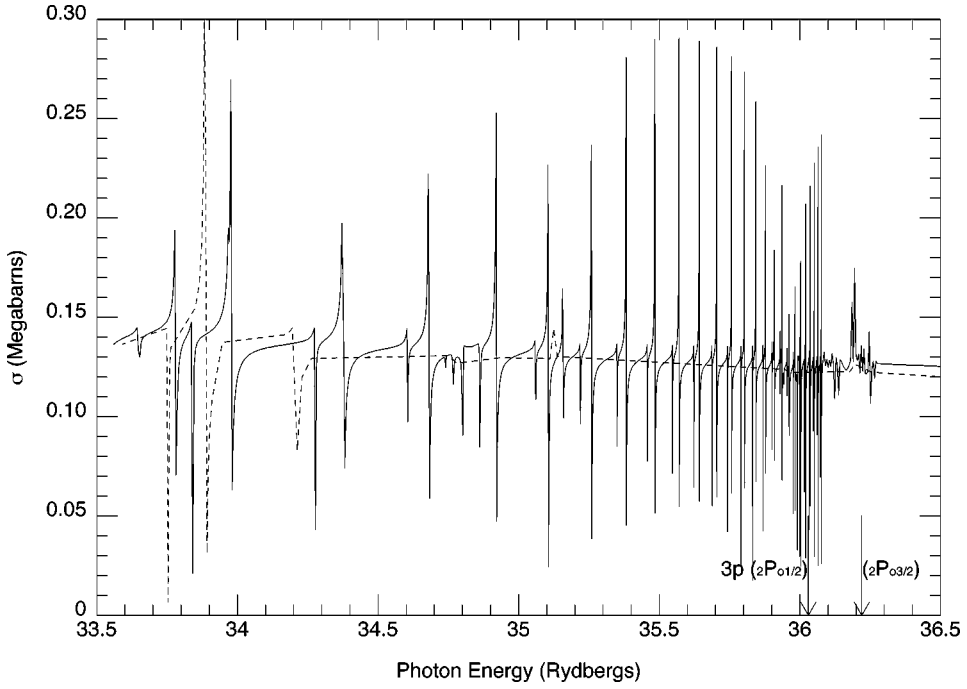

FIG. 1. Photoionization cross section of the ground level of Fe XV $3s^2(^1S_0)$ in the near-threshold region; solid line, relativistic BPRM results; dashed line, nonrelativistic results (OP [8]).

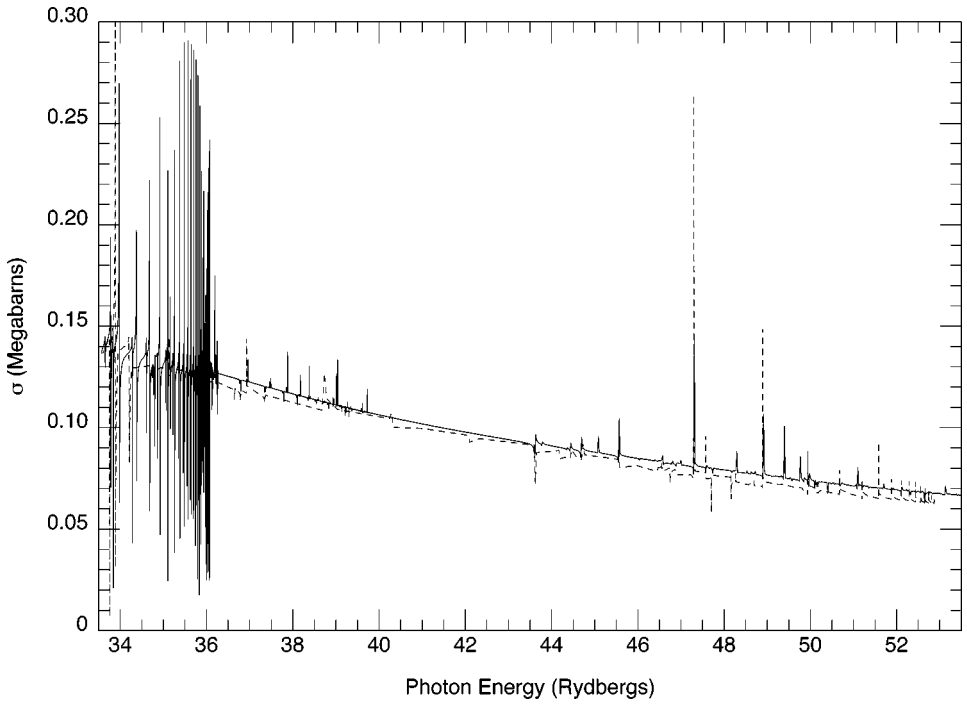

FIG. 2. Comparison of the present BPRM cross sections with the earlier OP nonrelativistic calculations over an extended range spanning all target thresholds in the close-coupling expansion.

Finally, Fig. 4 shows the complete set of BPRM and RMQDT+RRPA results obtained. The strongest resonances in the middle range between 54 and 70 Ry correspond mainly to inner-shell excitation configurations $2p^5 3s^2(3p,3d)$, particularly to the $2p \rightarrow 3d$ excitation. We identify these resonances from an extensive atomic-structure configuration-interaction calculation for Fe XV using SUPERSTRUCTURE, employing the same one-electron orbital basis set as the target ion Fe XVI. For example, the autoionizing levels $2p^5 3s^2 3p[^{3,1}(S_1, P_{0,1,2}, D_{0,1,2,3})]$ lie between 54.49 and 56.83 Ry. The large resonance complex between 58.26 and 59.76 Ry corresponds to the autoionizing levels $2p^5 3s^2 3d[^{3,1}(S_1, P_{0,1,2}, D_{0,1,2,3})]$. The experimental first ionization potential of Fe XV is 33.58 Ry (the present BPRM calculated value is 33.56 Ry), and the highest Fe XVI target threshold is at 25.41 Ry. This implies that the *L*-shell resonance complex just below 60 Ry coincides with the highest target levels $5d(^2D_{3/2,5/2})$ in the wave-function expansion (Table I). It is clear that the inner-shell photoexcitation autoionization would be a major contributor to the effective photoionization cross sections *below* the *L*-shell ionization threshold(s).

The RRPA and RMQDT results in Figs. 3 and 4 show an excellent match with the background BPRM cross sections. The resonances just below the $2p$ ionization threshold form a pseudocontinuum whose effective area corresponds to the

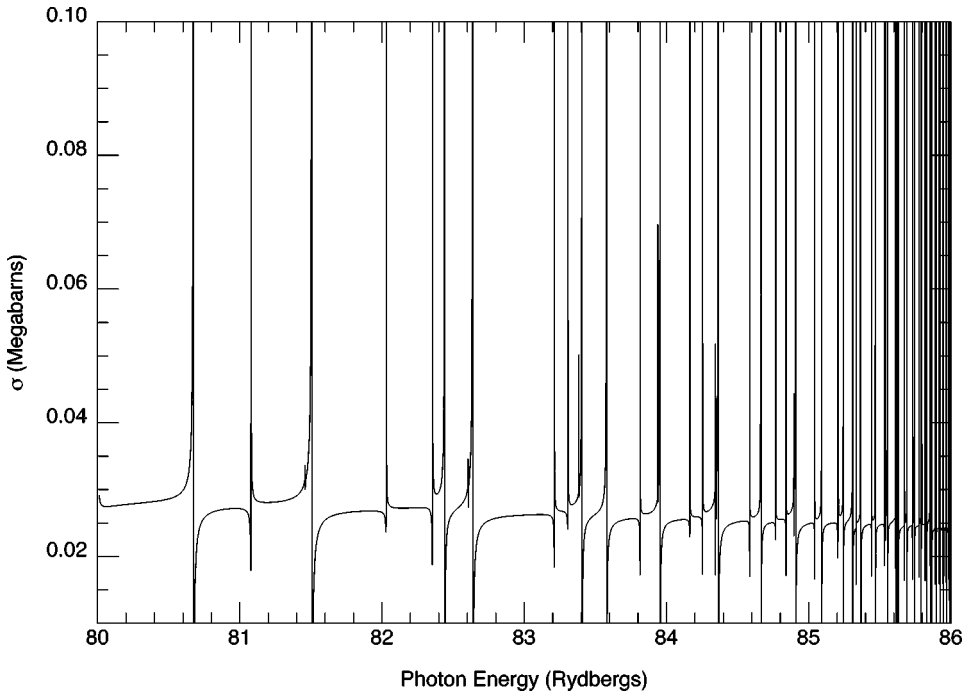

FIG. 3. RRPA and RMQDT cross sections with resonances converging on to the *L*-shell ionization thresholds.

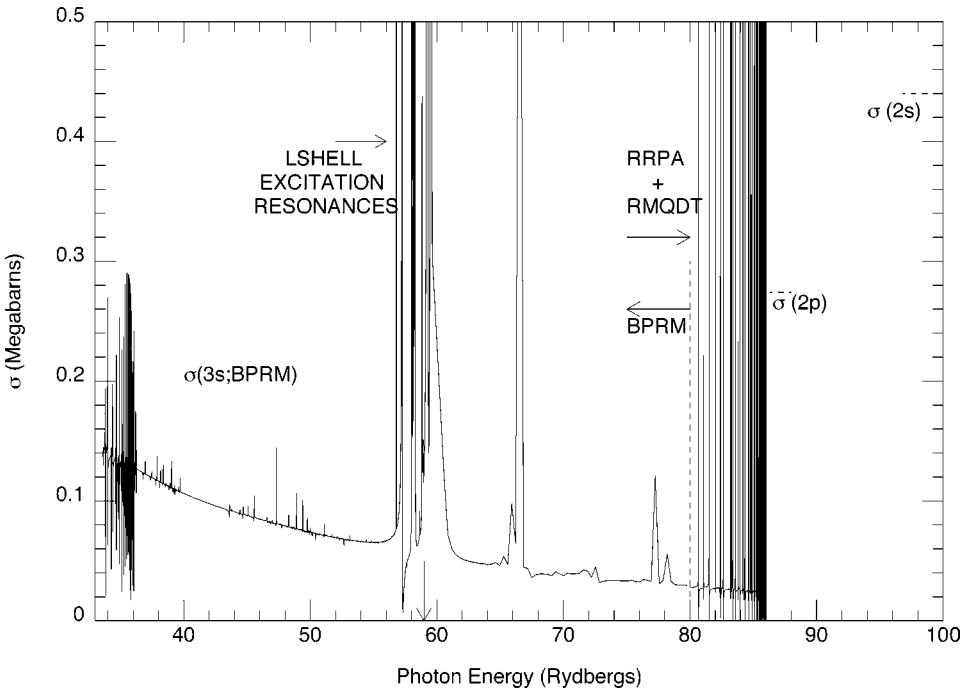

FIG. 4. The BPRM and (RRPA+RMQDT) cross sections in the energy range up to *L*-shell ionization. The arrow at 59.98 Ry is the highest target threshold in the BPRM calculations. The total subshell photoionization cross sections $\sigma(2p)$ and $\sigma(2s)$ are computed using the RRPA.

total photoabsorption in this region, which in turn rises to the threshold value at the $2p$ ionization energy of 86.26 Ry. The total photoabsorption cross section should be continuous across ionization thresholds. Therefore the cross section at and above threshold(s) is, in principle, comparable in magnitude to the effective resonance averaged photoexcitation-autoionization cross section below threshold(s). The energy region up to the $2p$ and $2s$ ionization thresholds in Fig. 4 is dominated by resonance structures, many of which are not yet considered. The inner-shell ionization edges in particular are not sharp jumps, as often obtained in nonresonant calculations, but as diffuse pseudocontinua rising up to the relevant threshold cross sections.

As these first detailed calculations including relativistic and resonance effects show, the BPRM close-coupling calculations with the large number of levels and channels in the intermediate-energy range should considerably enhance the photoionization cross section of Fe XV. Thus, calculations that neglect the extensive inner-shell excitation resonances are likely to underestimate the cross sections by large factors (as has been shown, for example, in the case of photoionization of neutral iron [10]). Although likely to be much more extensive, the present work emphasizes the urgent need for more elaborate BPRM calculations leading up to the *L*- and *K*-shell ionization thresholds, as these data would be essential requirements for photoionization modeling of astrophysical x-ray sources observed by CXO, XMM, and Astro-E.

This work was partially supported by the National Science Foundation and the NASA Astrophysical Theory Program. N.H. would like to thank Professor Walter Johnson for the use of his RRPA and RMQDT codes.

[1] T.R. Kallman, D. Liedahl, A. Osterheld, W. Goldstein, and S. Kahn, Astrophys. J. **465**, 994 (1996); P. Beiersdorfer, J.K. Lepson, G.V. Brown, S.B. Utter, S.M. Kahn, D.A. Liedahl, and C.W. Mauche, *ibid.* **519**, L185 (1999).

[2] R.F. Reilman and S.T. Manson, Astrophys. J., Suppl. **40**, 815 (1979); D.A. Verner, D.G. Yakovlev, I.M. Band, and M.B. Trzhaskovskaya, At. Data Nucl. Data Tables **55**, 233 (1993).

[3] M.J. Seaton, Y. Yu, D. Mihalas, and A.K. Pradhan, Mon. Not. R. Astron. Soc. **266**, 805 (1994); K.A. Berrington, P.G. Burke, K. Butler, M.J. Seaton, P.J. Storey, K.T. Taylor, and Y. Yu, J. Phys. B **20**, 6379 (1987).

[4] D.G. Hummer, K.A. Berrington, W. Eissner, A.K. Pradhan, H.E. Saraph, and J.A. Tully, Astron. Astrophys. **279**, 298 (1993); K.A. Berrington, W.B. Eissner, P.H. Norrington, Comput. Phys. Commun. **92**, 290 (1995).

[5] K.A. Berrington, L. Quigley, and H.L. Zhang, J. Phys. B **30**, 5409 (1997).

[6] H.L. Zhang, Phys. Rev. A **57**, 2640 (1998).

[7] W. Eissner, M. Jones, and H. Nussbaumer, Comput. Phys. Commun. **8**, 270 (1974).

[8] K. Butler, C. Mendoza, and C.J. Zeippen, J. Phys. B **26**, 4409 (1993).

[9] W.R. Johnson, C.D. Lin, K.T. Cheng, and C.M. Lee, Phys. Scr. **21**, 409 (1980).

[10] W.R. Johnson and K.T. Cheng, Phys. Rev. A **20**, 978 (1979).